AEDC-TR-75-97

EXPERIMENTS TO ASSESS THE INFLUENCE OF CHANGES IN THE TUNNEL WALL BOUNDARY LAYER ON TRANSONIC WALL CROSSFLOW CHARACTERISTICS

VON KÁRMÁN GAS DYNAMICS FACILITY
ARNOLD ENGINEERING DEVELOPMENT CENTER
AIR FORCE SYSTEMS COMMAND
ARNOLD AIR FORCE STATION, TENNESSEE 37389

November 1975

Final Report for Period November 1974 — January 1975

Prepared for

ARNOLD ENGINEERING DEVELOPMENT CENTER (DY)
AIR FORCE SYSTEMS COMMAND
ARNOLD AIR FORCE STATION, TENNESSEE 37389

NOTICES

When U. S. Government drawings specifications, or other data are used for any purpose other than a definitely related Government procurement operation, the Government thereby incurs no responsibility nor any obligation whatsoever, and the fact that the Government may have formulated, furnished, or in any way supplied the said drawings, specifications, or other data, is not to be regarded by implication or otherwise, or in any manner licensing the holder or any other person or corporation, or conveying any rights or permission to manufacture, use, or sell any patented invention that may in any way be related thereto.

Qualified users may obtain copies of this report from the Defense Documentation Center.

References to named commercial products in this report are not to be considered in any sense as an endorsement of the product by the United States Air Force or the Government.

This report has been reviewed by the Information Office (OI) and is releasable to the National Technical Information Service (NTIS). At NTIS, it will be available to the general public, including foreign nations.

APPROVAL STATEMENT

This technical report has been reviewed and is approved for publication.

FOR THE COMMANDER

CARLOS TIRRES
Captain, USAF
Research & Development
Division
Directorate of Technology

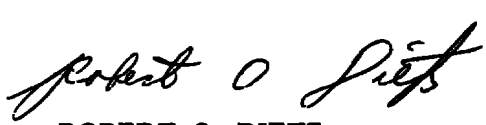

ROBERT O. DIETZ
Director of Technology

REPORT DOCUMENTATION PAGE	READ INSTRUCTIONS BEFORE COMPLETING FORM
1. REPORT NUMBER AEDC-TR-75-97	2 GOVT ACCESSION NO.
3. RECIPIENT'S CATALOG NUMBER	
4 TITLE (and Subtitle) EXPERIMENTS TO ASSESS THE INFLUENCE OF CHANGES IN THE TUNNEL WALL BOUNDARY LAYER ON TRANSONIC WALL CROSSFLOW CHARACTERISTICS	5 TYPE OF REPORT & PERIOD COVERED Final Report - November 1974 - January 1975
	6. PERFORMING ORG. REPORT NUMBER
7 AUTHOR(s) R. F. Starr, ARO, Inc.	8 CONTRACT OR GRANT NUMBER(s)
9 PERFORMING ORGANIZATION NAME AND ADDRESS Arnold Engineering Development Center(DY) Air Force Systems Command Arnold Air Force Station, Tenn. 37389	10 PROGRAM ELEMENT, PROJECT, TASK AREA & WORK UNIT NUMBERS Program Element 65807F
11 CONTROLLING OFFICE NAME AND ADDRESS Arnold Engineering Development Center(DYFS) Air Force Systems Command Arnold Air Force Station, Tenn. 37389	12. REPORT DATE November 1975 13 NUMBER OF PAGES 30
14 MONITORING AGENCY NAME & ADDRESS(if different from Controlling Office)	15 SECURITY CLASS. (of this report) UNCLASSIFIED 15a. DECLASSIFICATION/DOWNGRADING SCHEDULE N/A

16 DISTRIBUTION STATEMENT (of this Report)

Approved for public release; distribution unlimited.

17 DISTRIBUTION STATEMENT (of the abstract entered in Block 20, if different from Report)

18 SUPPLEMENTARY NOTES

Available in DDC

19 KEY WORDS (Continue on reverse side if necessary and identify by block number)

transonic wind tunnels pressure distribution
boundary layer
Reynolds number
conical bodies

20 ABSTRACT (Continue on reverse side if necessary and identify by block number)

The equivalent porosity of the test section wall in a transonic wind tunnel with a fixed geometric porosity and varying wall boundary-layer displacement thickness, δ^*, has been investigated. Previous experiments have demonstrated that the boundary-layer displacement thickness on the wall influences the wall crossflow characteristic. Experimental data from a Ludwieg tube type of transonic tunnel are compared with data from conventional transonic

DD FORM 1 JAN 73 1473 EDITION OF 1 NOV 65 IS OBSOLETE

20. ABSTRACT (Continued)

tunnels in the Mach number range from 0.95 to 1.15. The displacement thickness studied is comparatively thin and represents typical values which will be encountered in future high Reynolds number transonic tunnels. Based on the change in static pressure measured on a cone-cylinder model, it is shown that a factor of two variation in the tunnel wall δ^* results in an equivalent wall porosity change of less than one percent in the range $0.13 \leq \delta^*/d \leq 0.28$, where d is the wall hole diameter.

AFSC
Arnold AFS Tenn

PREFACE

The work reported herein was conducted by the Arnold Engineering Development Center (AEDC), Air Force Systems Command (AFSC), under Program Element 65807F. The research was conducted from November 1974 through January 1975 by ARO, Inc. (a subsidiary of Sverdrup & Parcel and Associates, Inc.), contract operator of AEDC, AFSC, Arnold Air Force Station, Tennessee, under ARO Project No. V37A-32A. The author of this report was R. F. Starr, ARO, Inc. The manuscript (ARO Control No. ARO-VKF-TR-75-45) was submitted for publication on April 29, 1975.

CONTENTS

Page

1.0 INTRODUCTION 5
2.0 EXPERIMENTAL APPARATUS
2.1 Pilot Transonic Tunnel, Pilot HIRT 7
2.2 Instrumentation 9
2.3 Cone-Cylinder Model and Boundary-Layer Rake 10
3.0 PROCEDURE
3.1 General 11
3.2 Tunnel Calibration 13
3.3 Tunnel Wall Boundary-Layer Characteristics 14
4.0 RESULTS AND DISCUSSION
4.1 Mach 0.95 18
4.2 Porosity Sensitive Conditions 19
4.3 Quantifying the Results 21
5.0 CONCLUSIONS 22
REFERENCES 28

ILLUSTRATIONS

Figure

1. Influence of Boundary-Layer Displacement Thickness on Crossflow Characteristics of Perforated Wall with 60-deg Inclined Holes, Hole Diameter 1/8-in., Wall Thickness 1/8 in., Open-Area Ratio 6 percent at $M_\infty = 1.2$ 6
2. Sketch of AEDC/VKF Pilot HIRT Facility 7
3. Details of Pilot HIRT Facility 8
4. Pilot HIRT Plenum Exhaust System 9
5. Installation Drawing of the Cone-Cylinder, Boundary-Layer Rake, and Differential Pressure Transducers, Pilot HIRT 10
6. Photograph of the Cone-Cylinder and Boundary-Layer Rake Installed in Pilot HIRT 11
7. Approximate Locations of Reflected Wave Disturbances upon a 1-percent Blockage, 20-deg Cone-Cylinder Model in a Square Tunnel 12
8. Variation of Stagnation Pressure, Plenum Static Pressure, and Selected Cone-Cylinder Static Pressures with Time in a Pilot HIRT Run at $M_\infty = 1.096$, $P_o = 110$ psia 13

Figure | Page

9. Tunnel Centerline Static Calibration Results, Pilot HIRT 14
10. Boundary-Layer Characteristics at the Center of Model Rotation in Pilot HIRT 15
11. Comparison of Cone-Cylinder Pressure Distribution Data at Mach Number 0.95 Obtained from Various Facilities 18
12. Cone-Cylinder Pressure Distributions at Mach Numbers of 1.05 to 1.15 for a Range of Stagnation Pressures 20
13. Comparison of Cone-Cylinder Pressure Distribution Data at Mach Numbers of 1.05 to 1.15 at Various Flow Times in Pilot HIRT 23
14. Cone-Cylinder Pressure Distributions at Mach Numbers of 1.05 to 1.15 for Extremes of δ^*/d 26
15. Influence of Varying Wall Porosity on Cone-Cylinder Pressure Distributions (from Ref. 3) 27
16. Change in Cone-Cylinder Pressure Ratio with Porosity for Mach Numbers 1.05 to 1.10 28

NOMENCLATURE 29

1.0 INTRODUCTION

Currently, there is great interest in advanced high Reynolds number transonic facilities and several major development programs are underway in both the USA and Europe to investigate several different types of high Reynolds number transonic wind tunnels. Wall boundary-layer changes occur as the free-stream Reynolds number is varied in each type of tunnel under consideration, and the wall boundary-layer thichkness changes with time during the course of the run in some of the tunnel types.

In the test section of a transonic facility, flow properties at the semiopen tunnel wall play a first order role in establishing the correct aerodynamic flow over the model under test. The wall boundary condition, or wall crossflow characteristic, has been shown to be somewhat sensitive to the wall boundary-layer properties. Figure 1a, which is taken directly from Ref. 1, illustrates the variation in the wall crossflow characteristic, $dC_p/d\theta$, for changes in the boundary-layer displacement thickness, δ^*, under the constraints of that particular experiment ($\delta^*/d > 0.5$). These experimental results are presented in a slightly different form in Fig. 1b which illustrates that a factor of two change in δ^*, for a given hole diameter, produces nearly a 50-percent change in the wall crossflow characteristic. Comparing the trends shown in Fig. 1b with more recent wall crossflow data obtained in a tunnel having walls of variable porosity (Ref. 2 gives an expression for the variation of $dC_p/d\theta$ with wall porosity, τ_w, as $dC_p/d\theta = 5 - 5/12\ \tau_w$), it appears that this factor of two change in δ^* could be equivalent to a wall porosity change of about three percent which cannot be ignored based on the experimental work reported in Ref. 3. For transonic testing, then, special care must be taken to ensure that variations in model aerodynamics which appear with changing free-stream Reynolds number are not actually the result of an altered wall crossflow character or conversely that real Reynolds number variations on the model are not offset by wall crossflow changes (δ^* or τ_w induced).

The object of this study is to make a preliminary assessment of the sensitivity of wall crossflow parameters to changes in the tunnel wall boundary layer. The intent is to quantify any apparent boundary-layer-induced crossflow changes in terms of an equivalent wall porosity change. In particular, the crossflow properties present in Ludwieg tube type transonic tunnel were of primary interest because of the thick wall boundary layer that will exist. The Ludwieg tube transonic wind tunnel used in these experiments is described in Ref. 4. The wall boundary-layer thickness in a Ludwieg tube changes about a factor of two during the course of a tunnel run. To provide additional data the tunnel stagnation pressure was varied by a factor of four, thereby producing a basic 30-percent change in boundary-layer thickness at any given time during the run. The strength of waves generated by a cone-cylinder model, which reflect off of the tunnel wall and return to the model, was used as the primary indicator of wall boundary condition changes.

Detailed measurements of the tunnel wall boundary layer with and without the cone-cylinder installed, sidewall static pressure measurements, and a careful centerline static calibration were made at many test conditions.

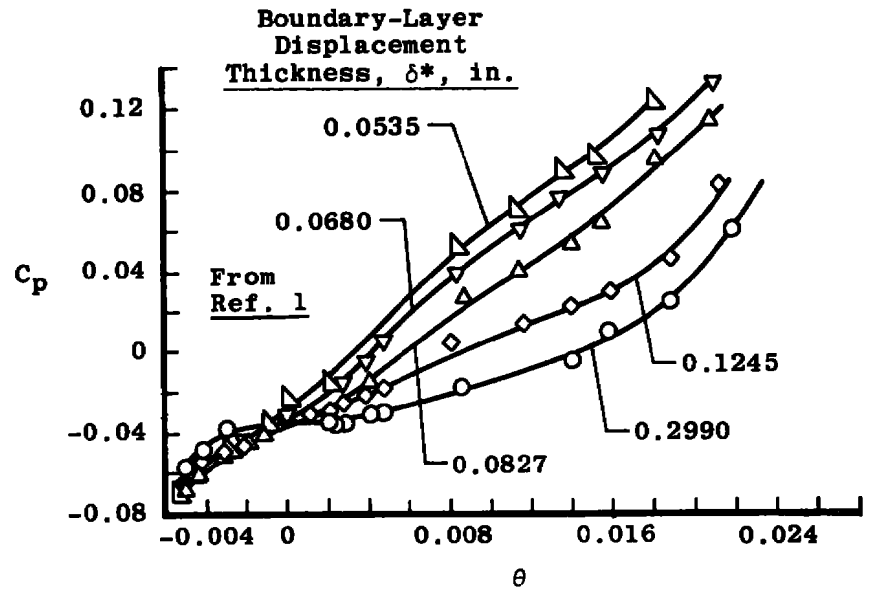

a. Wall pressure coefficient as a function of the flow angle at the wall for a range of δ*

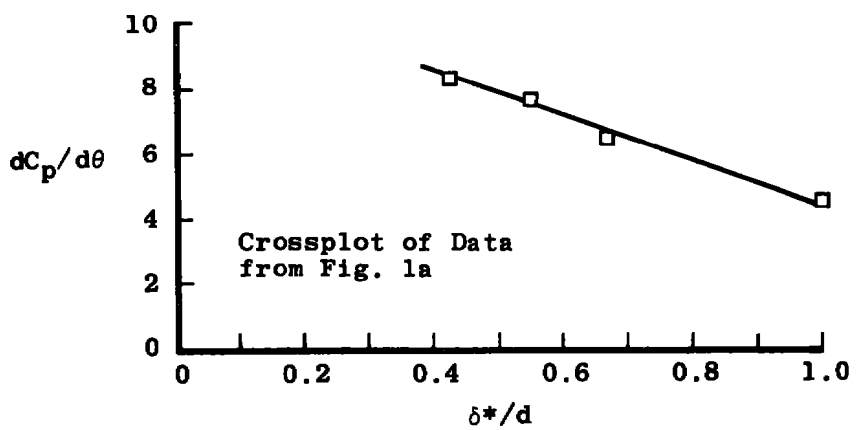

b. Wall crossflow characteristic as a function of δ*/d

Figure 1. Influence of boundary-layer displacement thickness on crossflow characteristics of perforated wall with 60-deg inclined holes, hole diameter 1/8 in., wall thickness 1/8 in., open-area ratio 6 percent at M_∞ = 1.2.

2.0 EXPERIMENTAL APPARATUS

2.1 PILOT TRANSONIC TUNNEL, PILOT HIRT

The AEDC-VKF Pilot High Reynolds Number Facility (Pilot HIRT) is a laboratory-scale model of a high Reynolds number transonic facility. A schematic drawing of the tunnel is given in Fig. 2. This facility can be charged to 800 psia which produces a maximum stagnation pressure of about 500 psia in the transonic speed range. The Ludwieg

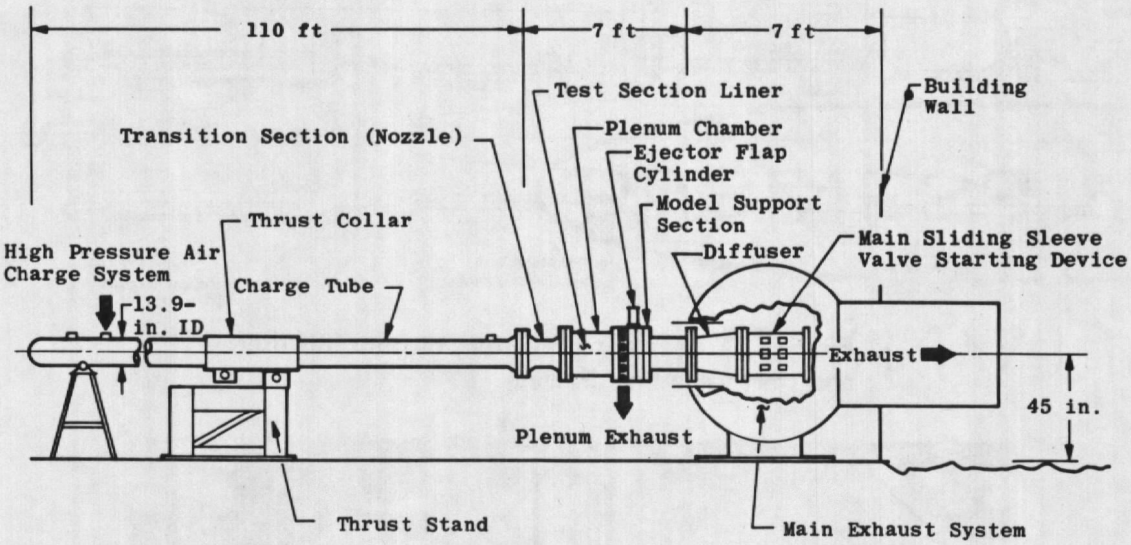

Figure 2. Sketch of AEDC/VKF Pilot HIRT facility.

tube storage system (charge tube) is 13.9 in. in diameter and is 110 ft long. A transition section with a contraction ratio of 2.25 channels the flow from the circular charge tube into a rectangular test section which is 7.3 by 9.15 in. The test section-plenum chamber is shown in more detail in Fig. 3. The porous walls are of conventional design with 60-deg inclined holes. The porosity can be varied manually by moving one porous plate relative to another (two plates constitute a wall). When the holes are fully aligned, the porosity is ten percent. The cutoff plate motion is upstream to reduce porosity. An ejector flap section is located at the back of the porous plates. The flaps are on all four walls and can be set to a greater opening during the tunnel starting process and reduced to the desired setting during the steady run (Fig. 3). The plenum chamber which encloses the test section has a volume which is about 1.8 times the test section volume (neglecting the volume of the wall support structure). The plenum is exhausted directly to atmosphere through the choked orifice-valve system shown in Fig. 4. The desired auxiliary flow rate through the plenum system is obtained by adjusting the orifice and by opening or closing the quick-acting valve illustrated in Fig. 4. The plenum exhaust flow is initiated

by rupturing a diaphragm in the line. The volume of the plenum chamber and the plenum exhaust lines is about 2.5 times the test section volume. A model support section, diffuser, and main starting device are located downstream of the test section (see Fig. 3). A fast-acting sliding sleeve has been used as the main starting device in the tests which will be described. This valve opens in 20 to 30 msec. All of the exhaust air is channeled out of the building through the exhaust sphere (Fig. 2).

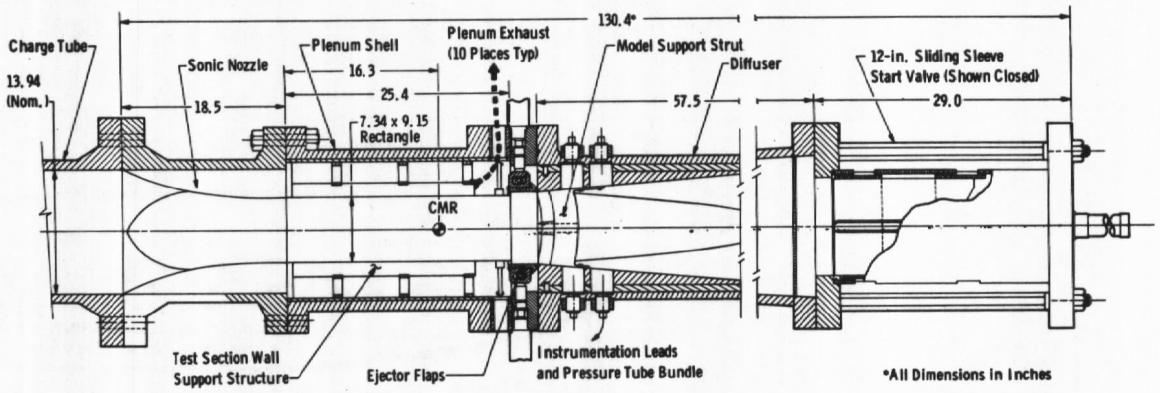

a. Pilot HIRT nozzle, test section, plenum, diffuser and start valve line drawing

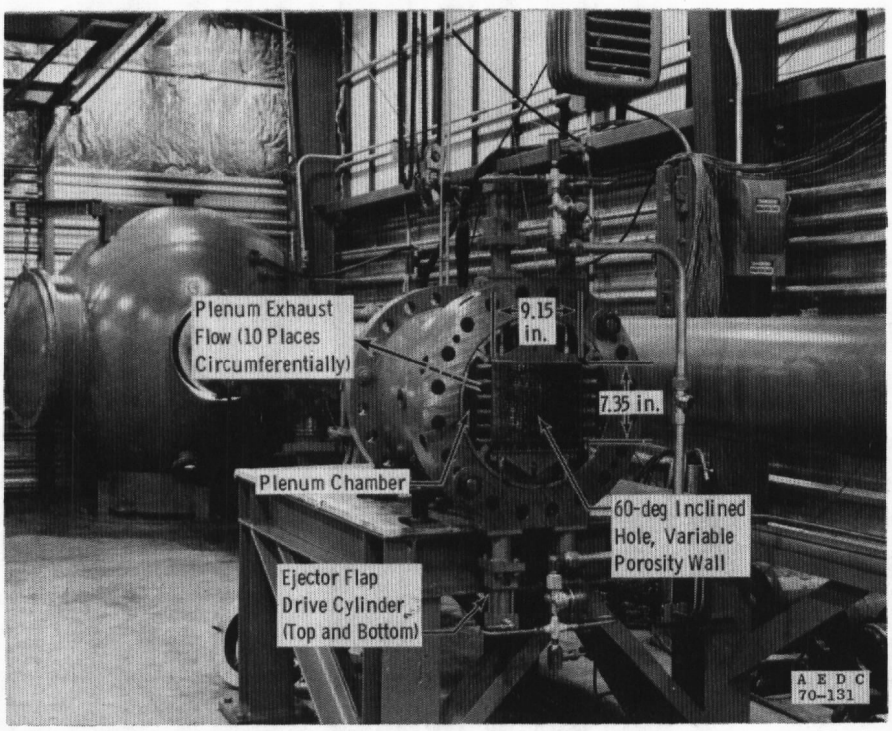

b. Photograph of the test section–plenum

Figure 3. Details of Pilot HIRT facility.

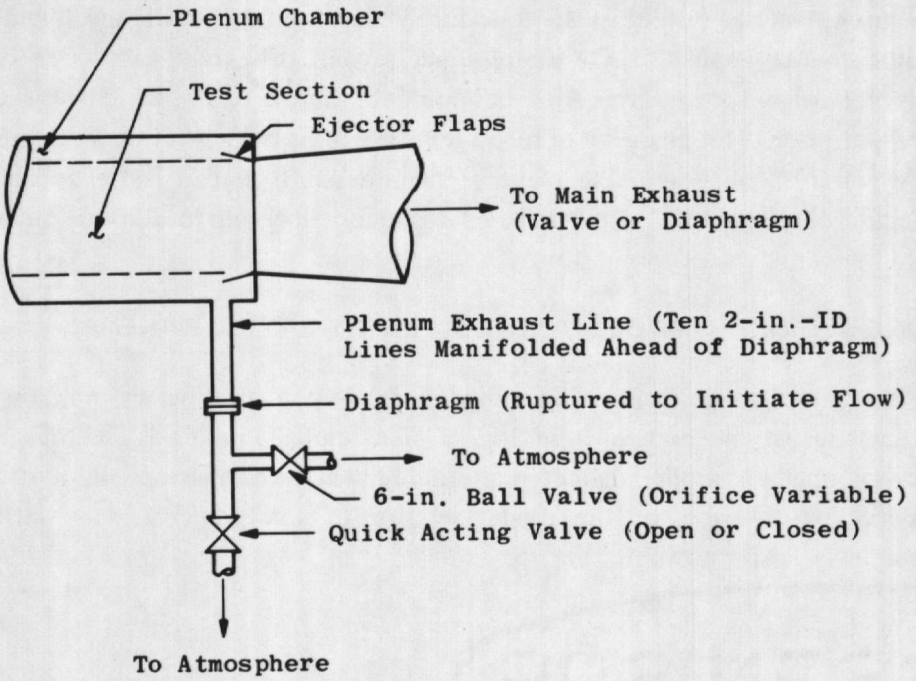

Figure 4. Pilot HIRT plenum exhaust system.

After the tunnel is pressurized to the desired pressure, a tunnel run is initiated by opening the main starting device. The plenum exhaust system is required for Mach numbers above 0.95. The duration of the first cycle of the run of this pilot tunnel is about 185 msec, and the tunnel starting process consumes the first 80 msec of this time. The duration of the steady portion of the run is about 100 msec. The tunnel operating conditions are established from a stagnation pressure measurement made in the charge tube just ahead of the nozzle and from a plenum chamber static pressure measurement made at the plenum shell wall near the center of model rotation.

2.2 INSTRUMENTATION

The pressure measurements during this series of experiments were obtained with small Kulite® semiconductor transducers. These transducers were located external to the tunnel and connected to the cone-cylinder model or the boundary-layer rake through tubes about 0.07 in. in diameter and 2 ft long. The tunnel-monitoring pressure measurements (stagnation and plenum pressures) were obtained similarly. The response time of these tubing configurations to a step input is about 20 msec at the pressures at which Pilot HIRT operates. A few test section wall pressure and tunnel monitoring pressure measurements were also obtained with the transducer located at the point of measurement to eliminate tube lag and provide a better measurement of pressure transient characteristics with time during the run.

The analog voltage output of the transducer was amplified, multiplexed, and converted to digital form at about 20,000 samples per second. The raw data were stored in a minicomputer for reduction after the run. One data sample was obtained on each channel about every 2 msec. The precision of measurement of this transducer-data recording system is better than 0.25 percent in the range of measurement on this test. The analog signals from selected channels were also paralleled to an oscillograph to allow a quick post-run evaluation of the data in visual form.

2.3 CONE-CYLINDER MODEL AND BOUNDARY-LAYER RAKE

A 20-deg total-angle, cone-cylinder model of 0.98-percent blockage was sting mounted at zero angle of attack as shown in Fig. 5. The model contained 18 pressure orifices spaced every one-half model diameter alternating between the top and bottom ray of the model. The location of the model relative to three tunnel wall static pressure measurements is also shown in Fig. 5.

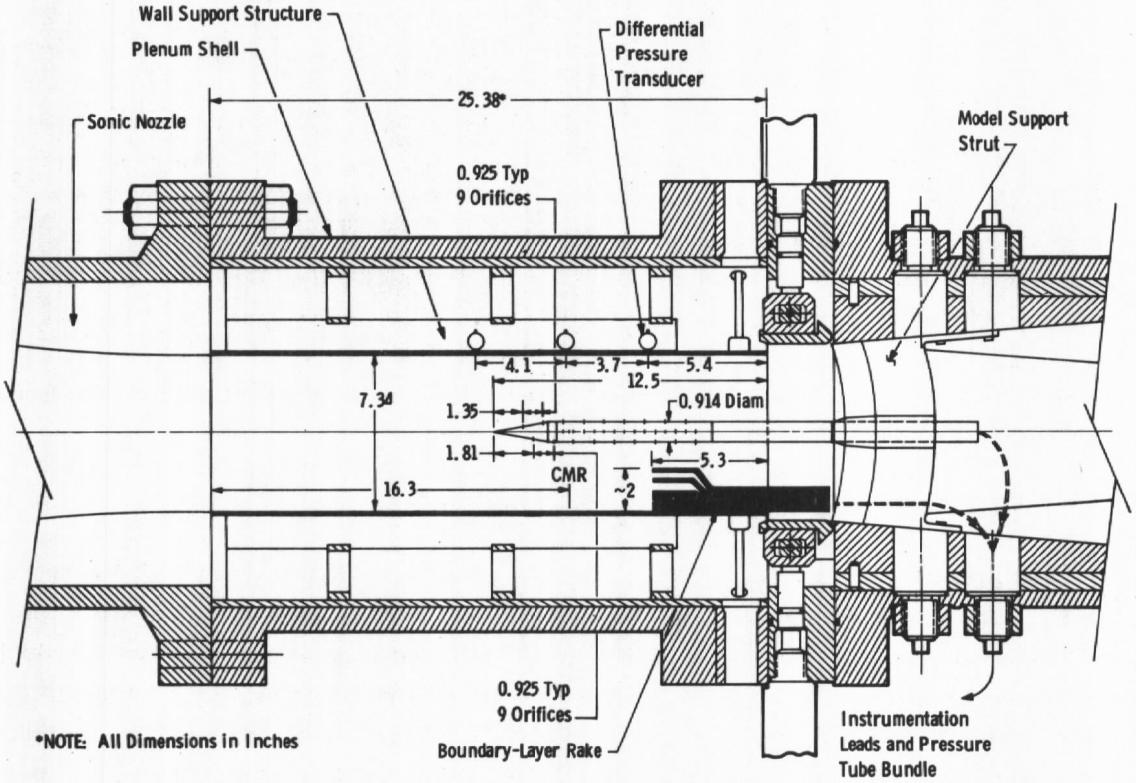

Figure 5. Installation drawing of the cone-cylinder, boundary-layer rake, and differential pressure transducers, Pilot HIRT.

A boundary-layer rake containing 12 total pressure probes spaced from the wall to about 2 in. above the wall was also used. The frontal blockage of this rake is less than 0.2 percent. The rake was located on the bottom wall of the tunnel at about x/D = 8 relative to the cone cylinder as shown in Fig. 5. An installation photograph of the cone-cylinder model and boundary-layer rake is shown in Fig. 6.

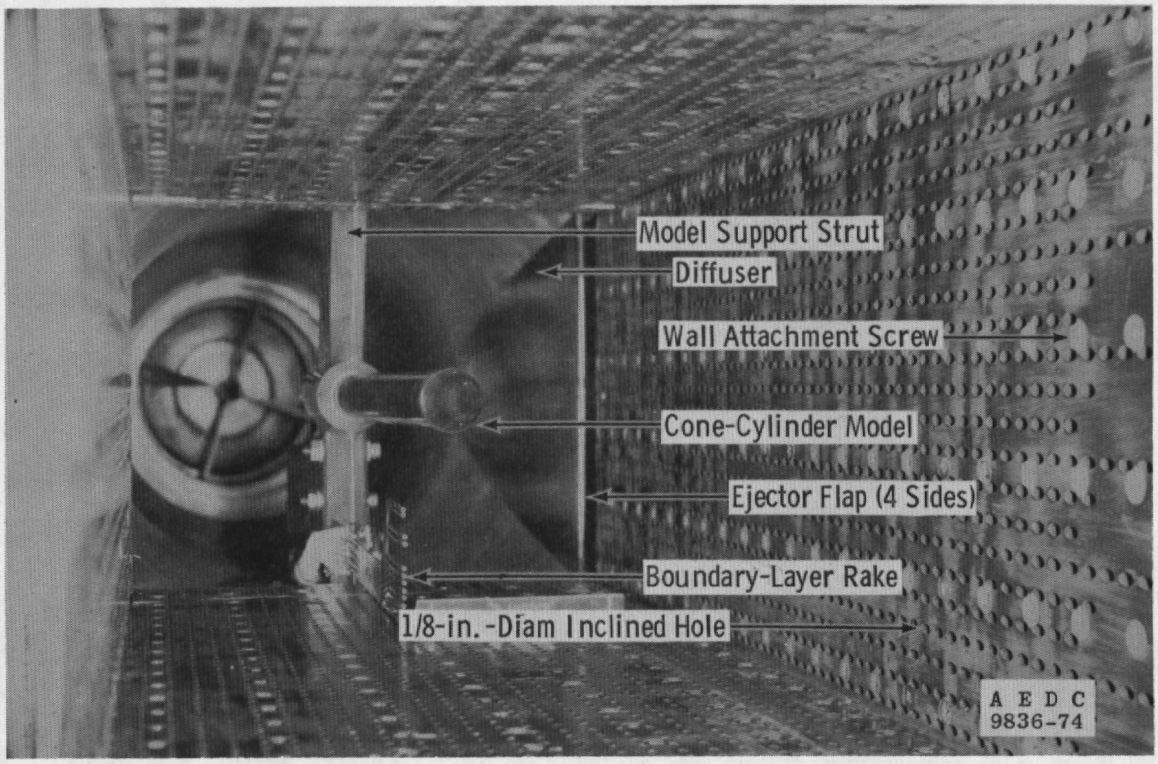

Figure 6. Photograph of the cone-cylinder and boundary-layer rake installed in Pilot HIRT.

3.0 PROCEDURE

3.1 GENERAL

This study involved utilizing a cone-cylinder model at transonic conditions for which discrete shock waves and expansion fields are generated by the model in a manner similar to the experiments of many other investigators (Refs. 1 and 3). These waves impinge on the tunnel test section porous wall where, depending on the boundary conditions at the wall, they are reflected as waves of the same family (wall too closed or restrictive to crossflow) or waves of the opposite family (wall too open or permissive to crossflow). The strength of the reflection is also very sensitive to the wall boundary condition. The supposition for this study is that relatively small changes in the wall boundary condition,

which might result from boundary-layer thickness variations, could be detected by changes in the strength or a change in the family of the reflected waves. A determination of the approximate source of the reflected wave can also be made based on characteristic flow-field solutions and experimental observations as given in Fig. 7 (Ref. 5).

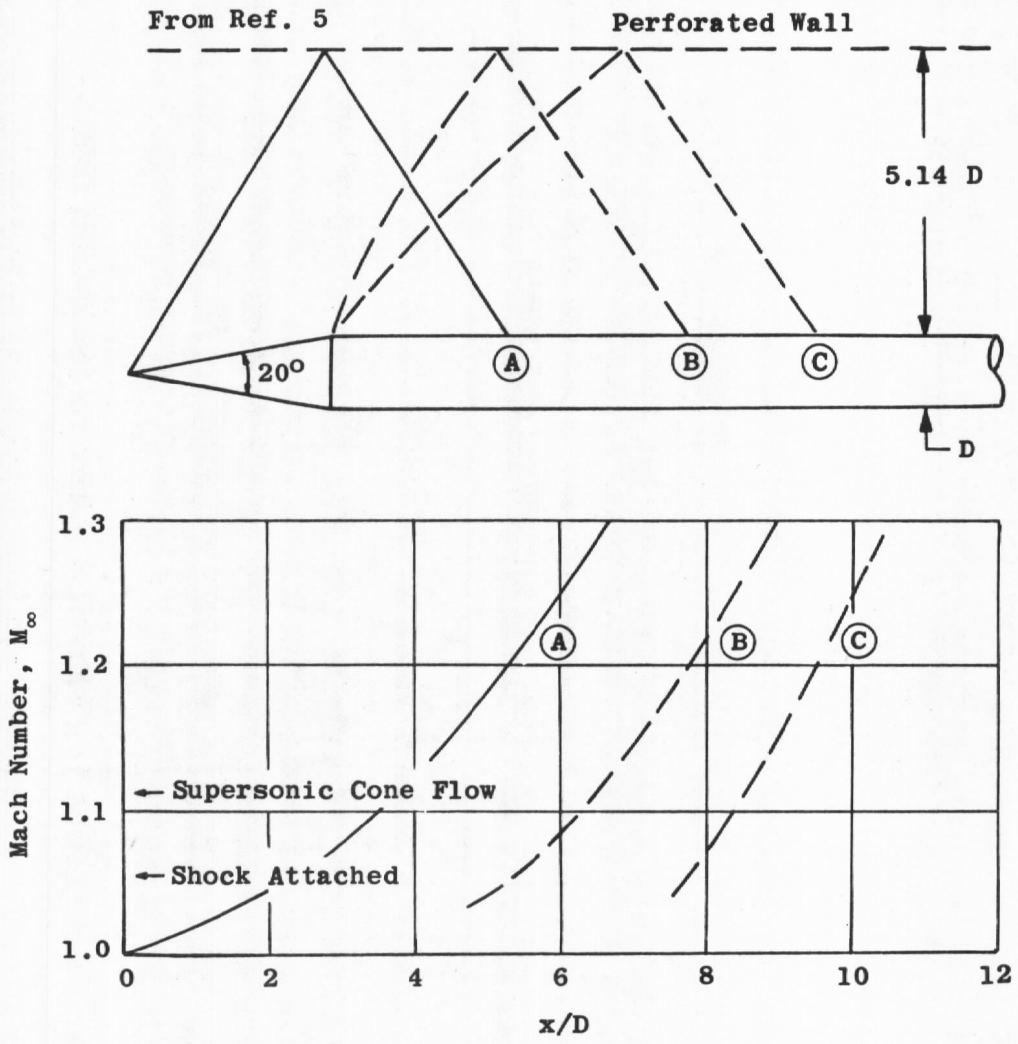

Figure 7. Approximate locations of reflected wave disturbances upon a 1-percent blockage, 20-deg cone-cylinder model in a square tunnel.

Pressure distribution data were obtained on the cone-cylinder model in the Mach range from 0.95 to 1.2 for stagnation pressures of 55, 110, and 220 psia. Runs were made for the three stagnation pressures at nearly identical Mach numbers to determine the influence of a unit Reynolds number change in the wall boundary layer on the apparent wall crossflow. Care was also taken to obtain a nearly constant Mach number from very early in a run to very late in a run to observe the influence of a wall boundary-layer

thickness change with time on the apparent wall crossflow. During this test the wall porosity was set at 4 percent and not varied. The ejector flaps were also held at a constant setting.

The variation of selected pressures during a typical run is illustrated in Fig. 8. At the completion of the tunnel starting process, the tunnel stagnation and plenum pressures remain constant within ±1/4 percent and the plenum Mach number, M_p, is invariant within 0.005.

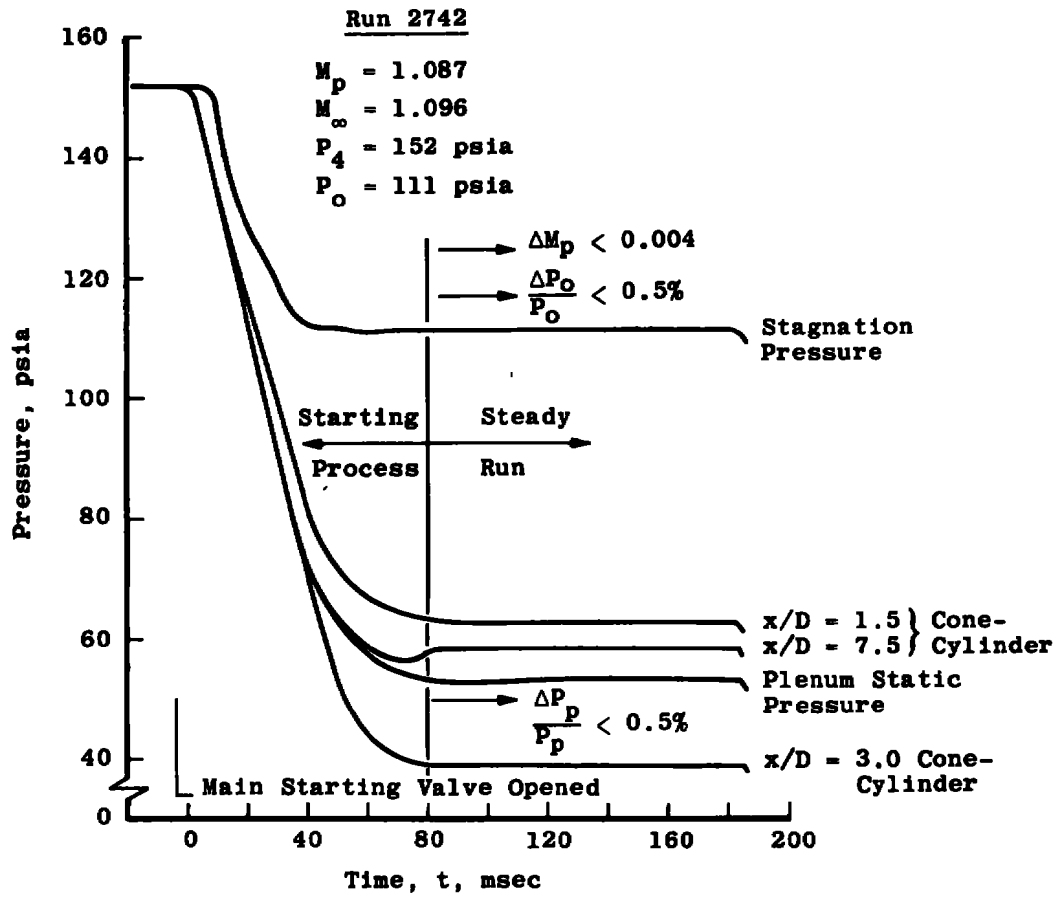

Figure 8. Variation of stagnation pressure, plenum static pressure, and selected cone-cylinder static pressures with time in a Pilot HIRT run at M_∞ = 1.096, P_o = 110 psia.

3.2 TUNNEL CALIBRATION

A centerline static pressure calibration of the pilot tunnel was repeated before this test to ensure that no significant variations with time during the run, or with stagnation pressure from run to run, occurred. The distribution of pressure along the test section

centerline was found to be invariant within the precision of measurement after the tunnel starting process ended and there were no measurable changes in the centerline distribution for the range of stagnation pressures tested. The difference between the plenum Mach number, M_p, and the average test section or free-stream Mach number, $\bar{M}_\infty$, was also nearly invariant after the tunnel started and for the range of stagnation pressures as shown in Fig. 9.

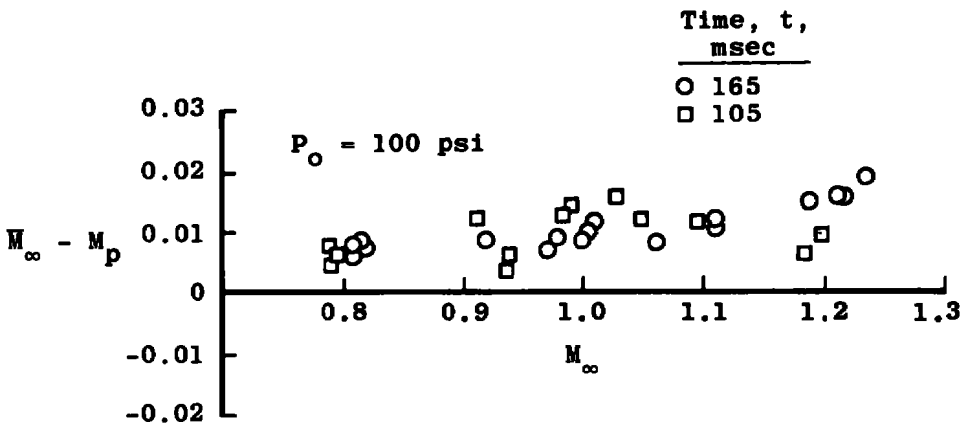

a. Mach number difference versus free-stream Mach number

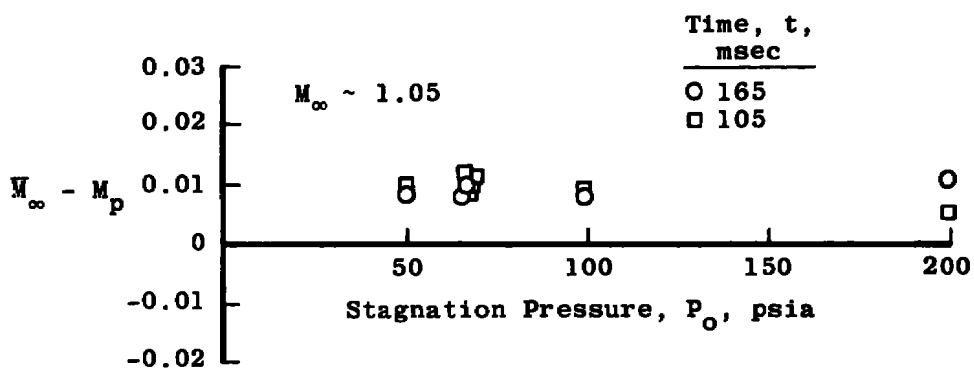

b. Mach number difference versus stagnation pressure

Figure 9. Tunnel centerline static calibration results, Pilot HIRT.

3.3 TUNNEL WALL BOUNDARY-LAYER CHARACTERISTICS

An accurate determination of the characteristics of the tunnel wall boundary layer for the various test conditions was essential for this study. The variation of the boundary-layer thickness, δ, and the displacement thickness, δ^*, with time during a Pilot HIRT run and with stagnation pressure is given in Figs. 10a and b. The boundary-layer

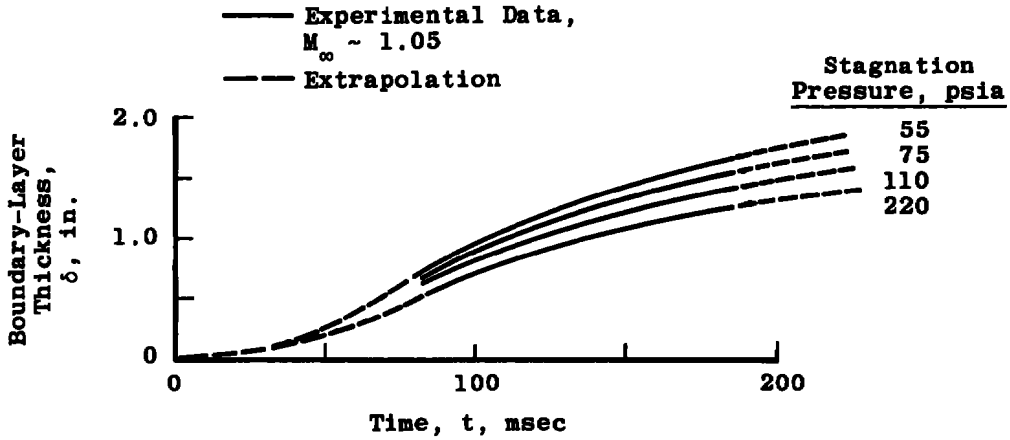

a. Boundary-layer thickness at the center of model rotation in Pilot HIRT for a range of stagnation pressures and times

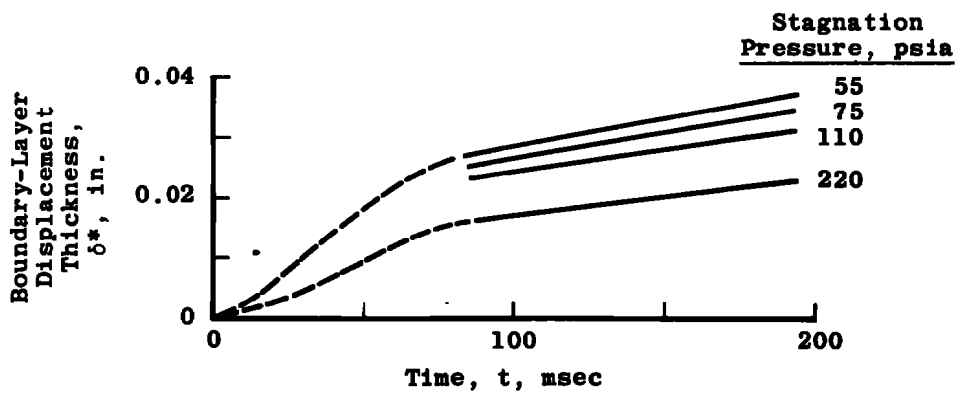

b. Displacement thickness at the center of model rotation in Pilot HIRT for a range of stagnation pressures and times

Figure 10. Boundary-layer characteristics at the center of model rotation in Pilot HIRT.

thickness is seen to increase about 100 percent from the earliest point at which cone-cylinder data will be discussed (t ~ 85 msec) to late in the pilot tunnel run (t ~ 165 msec) and to increase about 30 percent as the stagnation pressure is decreased by a factor of four. However, the displacement thickness does not increase as much, about 30 percent, during the same time interval and increases more, about 60 percent, for the pressure decrease.

This is attributable to the fact that the test section wall boundary layer actually is made up of two relatively distinct parts. A typical boundary-layer mass flux profile taken at the center of model rotation (see Fig. 5) is given in Fig. 10c. The inner part

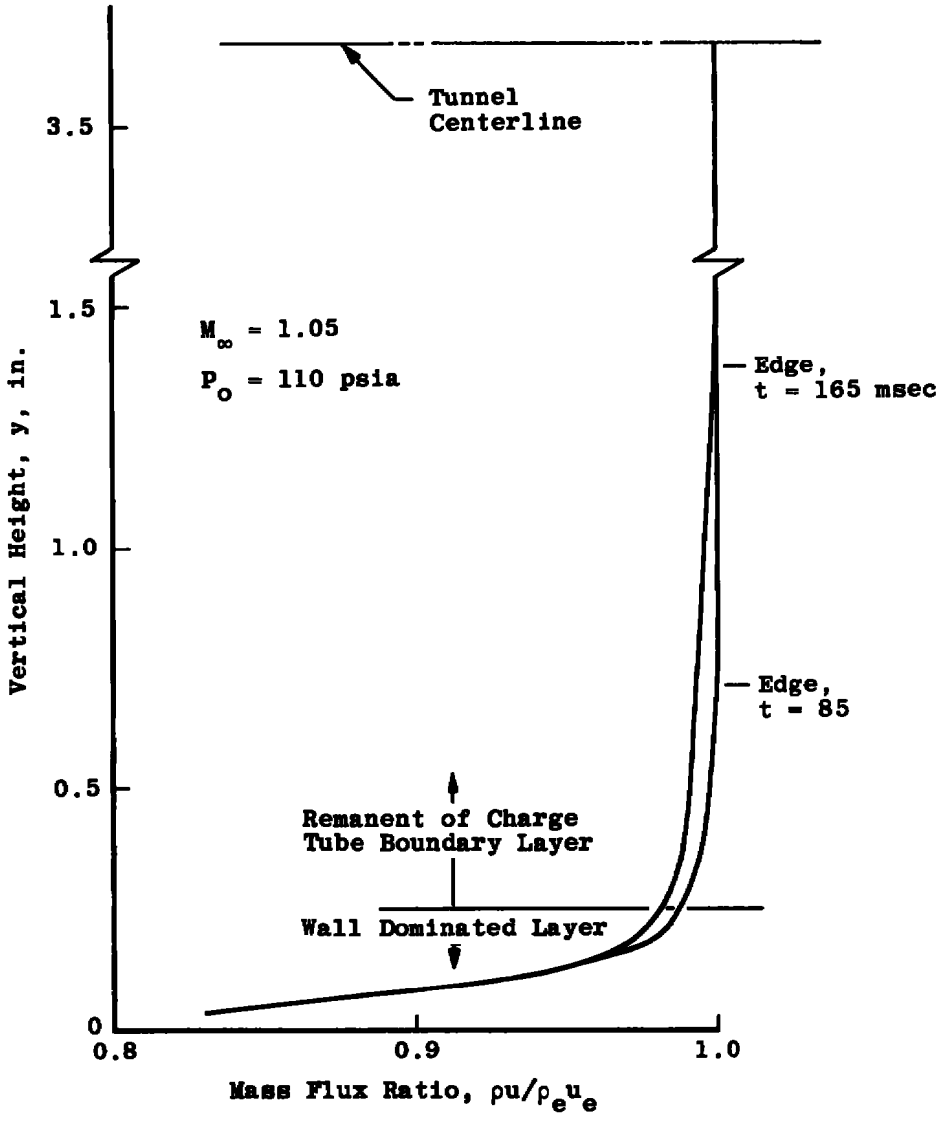

c. Boundary-layer mass flux profiles at the center of model rotation at times of 85 and 165 msec

Figure 10. Continued.

of the boundary layer ($y \lesssim 0.25$ in.) is the layer in which the velocity decrement has been imparted to the flow by the contoured contraction section and the test section wall itself. This part of the boundary layer is relatively invariant with time but does scale with unit Reynolds number changes (stagnation pressure), about like classical turbulent theories predict, and is the major contributor to the overall δ^* value. The outer part of the boundary layer is a layer in which the velocity decrement is imparted to the flow by the relatively thick turbulent boundary in the charge tube. This part of the boundary layer grows appreciably with time and also changes with unit Reynolds number, but has

a relatively smaller contribution to the δ^*. These statements about the various contributions to the overall δ^* are illustrated more graphically in Fig. 10d.

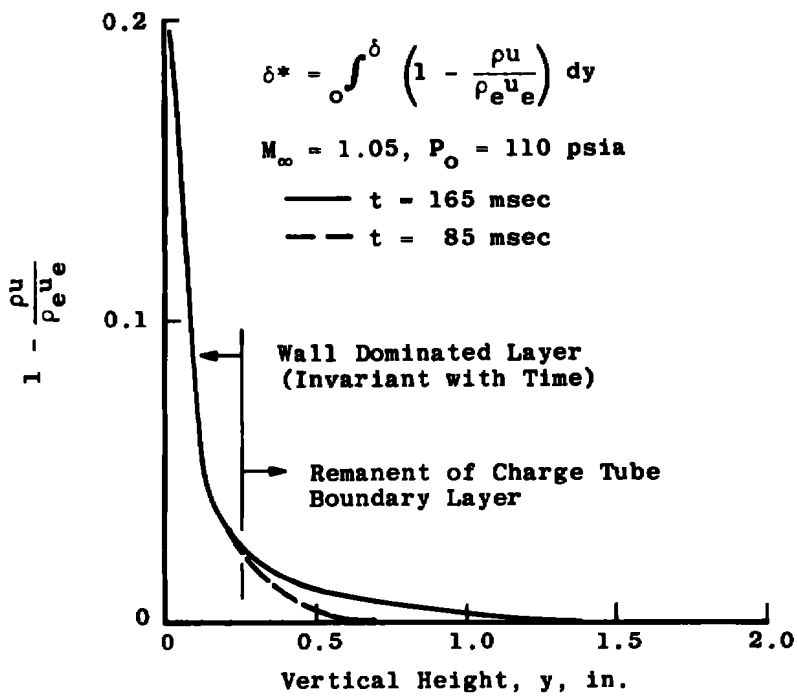

d. Displacement thickness integrand versus height
Figure 10. Concluded.

Finally, the character of the tunnel wall boundary layer was also checked with the cone-cylinder installed. Since the cone-cylinder imposes a rather severe pressure gradient on the wall, there was some concern that the boundary-layer trends with time and stagnation pressure determined in the tunnel empty tests might not apply with the cone-cylinder installed. Surprisingly, the boundary-layer trends with the cone-cylinder installed were found to be almost identical to those obtained with the tunnel empty at a cone-cylinder station eight body diameters from the nose of the cone (five diameters from the shoulder). Some work at the Arnold Engineering Development Center by R. L. Parker, ARO, Inc., has demonstrated that the wall boundary layer is altered right in the vicinity of the shoulder of the cone-cylinder where the waves are impinging on the wall and the localized pressure gradient exists ($x/D \sim 3$); however, this pressure gradient appears to produce only a local pertubation to the boundary layer. For the purposes of this study, the boundary-layer trends which have been determined with the tunnel empty or at an $x/D \sim 8$ with the cone-cylinder installed will be assumed to govern, even though the boundary layer in the region where the actual crossflow is dominant may be locally altered because of the model pressure field. It can only be assumed that the trends in boundary layer established in this fashion apply generally in the locally disturbed region.

4.0 RESULTS AND DISCUSSION

4.1 MACH 0.95

During the course of the cone-cylinder portion of the test, several runs were made at Mach 0.95 to assess model pressure orifice flushness and overall data quality. At this Mach number, all cylinder pressures downstream of x/D ~ 4.5 have been shown to be well behaved even for large variations in wall porosity at the one-percent blockage of this study. The results from several of these runs are given in Fig. 11. Figure 11a shows three runs at the maximum stagnation pressure of the test program for a nominal Mach number of 0.95. Experimental results from the AEDC 4-ft Transonic Wind Tunnel (4T) (Ref. 3) at the same one-percent blockage and approximately the same Mach number, as well as interference-free predictions, are given for comparison. The estimate of an interference-free trend presented in Ref. 3 is based on experimental data obtained in the AEDC 16-ft Transonic Wind Tunnel (16T) at 0.0625-percent blockage (Ref. 6) combined with theory where possible. Figure 11b shows similar results for the two extremes in stagnation pressure studied in this program.

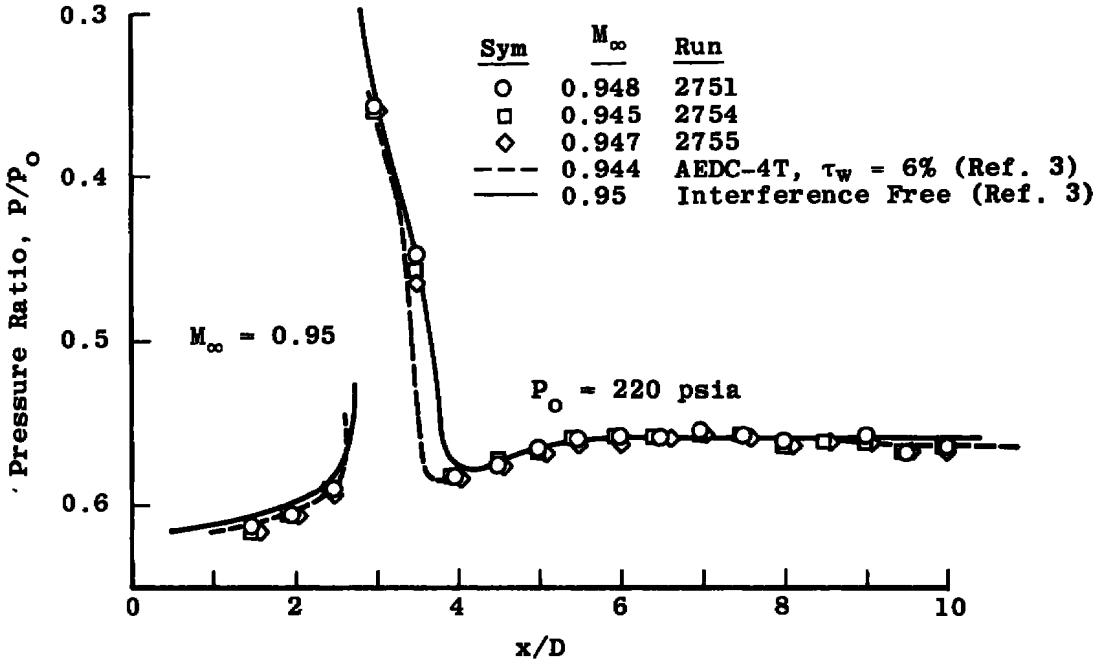

a. Mach number 0.95 at a stagnation pressure of 220 psia

Figure 11. Comparison of cone-cylinder pressure distribution data at Mach number 0.95 obtained from various facilities.

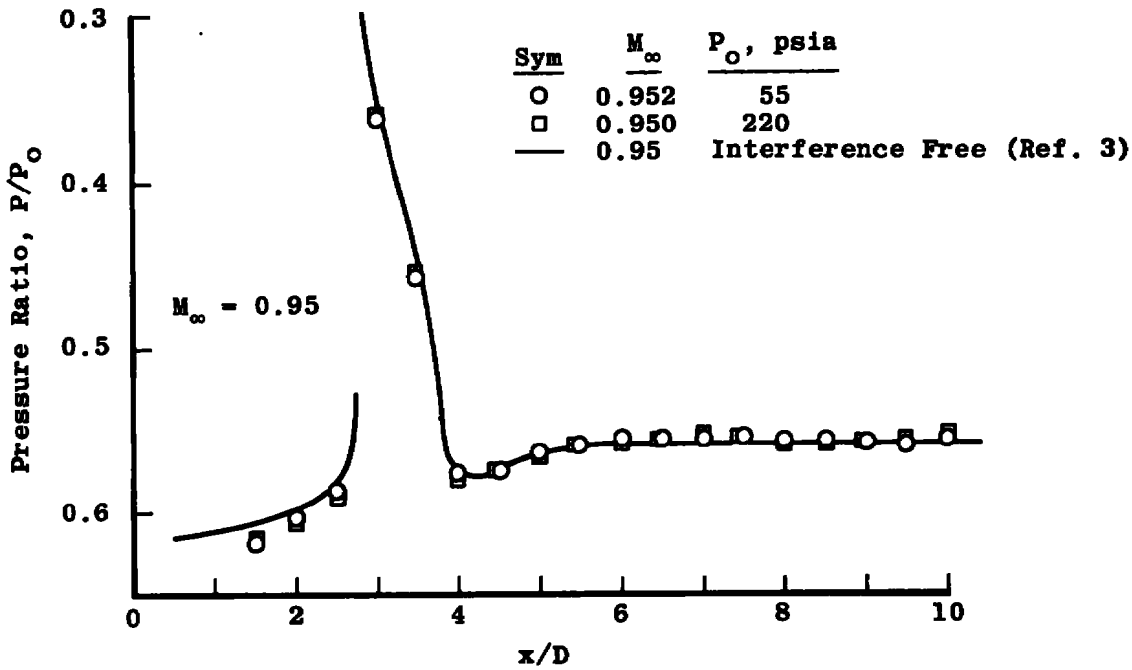

b. Mach number 0.95 at the two extremes in P_o

Figure 11. Concluded.

4.2 POROSITY SENSITIVE CONDITIONS

The principal effort in the program was directed toward studying the wall crossflow at conditions which have been demonstrated to be highly sensitive to wall porosity changes ($M_\infty \geqslant 1.05$) and for which regular, predictable, and quantifiable distortions in the model pressure distribution occur with porosity.

Figure 12 presents the results for nominal Mach numbers of 1.05, 1.075, 1.10, and 1.15 for stagnation pressures of 55, 110, and 220 psia. The δ^*/d variation at each Mach number is about 60 percent for this stagnation pressure range. All of these data are taken late in the tunnel run ($t \sim 165$ msec) such that no timewise δ^* variations are involved. It can be seen that the variations in the cone-cylinder pressure distribution with stagnation pressure are small. Part of this small variation is attributable to the Mach differences from one test condition to another ($\Delta M \lesssim 0.01$) and part may be attributable to slight effective porosity changes which will be quantified later. Interference-free results and comparable one-percent blockage results from Tunnel 4T are also presented for each Mach number. The one-percent blockage data from Tunnel 4T which are used for this comparison were taken at wall porosities of five and six percent. They are presented to illustrate the similarity in trends, but exact agreement is not expected because of differences in the ratio of the

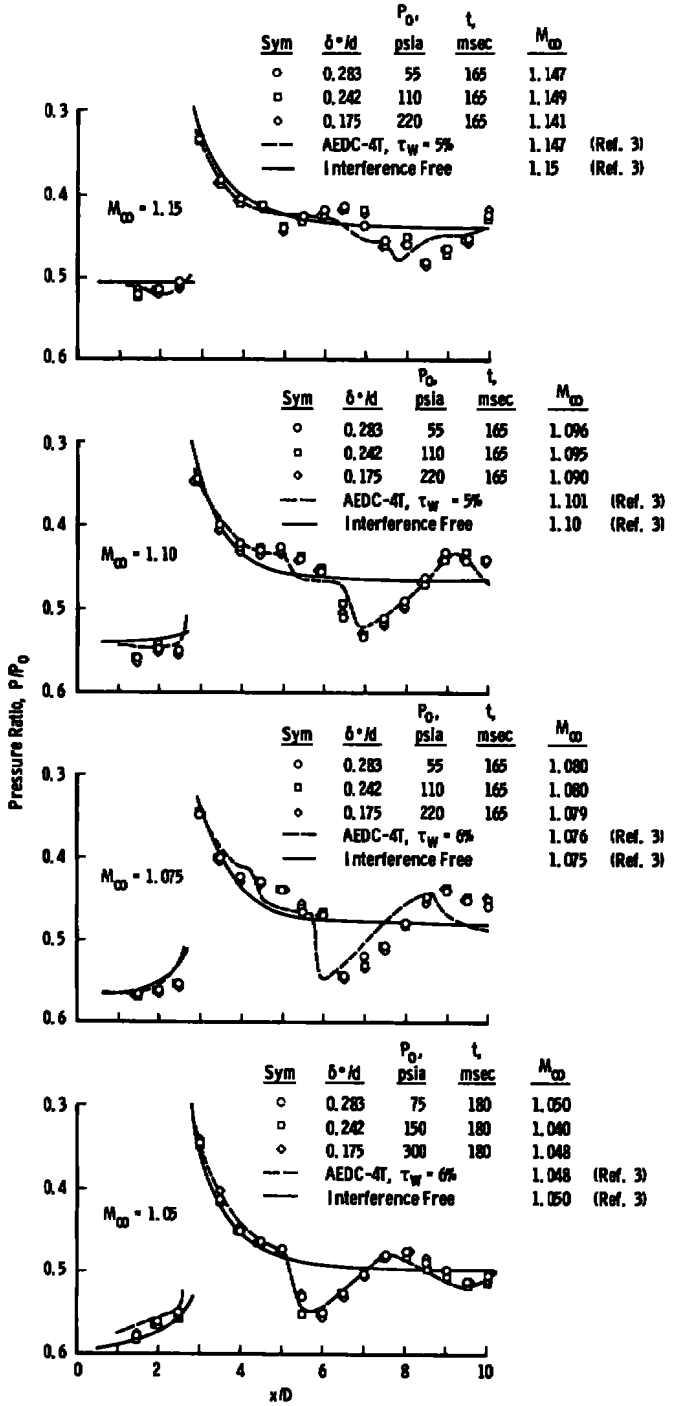

Figure 12. Cone-cylinder pressure distributions at Mach numbers of 1.05 to 1.15 for a range of stagnation pressures.

wall hole diameter to wall thickness, differences in test section geometry (rectangular versus square), and differences in wall hole pattern (inline hole pattern versus staggered hole pattern). In fact, all of the Pilot HIRT data taken at a wall porosity setting of four percent appear to agree more closely with the Tunnel 4T data taken at five or six percent than with the Tunnel 4T data taken at four percent.

Figure 13 presents the results for the same nominal Mach numbers as a function of boundary-layer growth with time at each of three stagnation pressures. In this case, the δ^* change from one test condition to another is about 25 to 30 percent. Again, the changes in cone-cylinder pressure distribution are slight and will be quantified in terms of effective porosity later.

Finally, the widest range of δ^*/d change which could be achieved in this experimental study comes by comparing data obtained early in a high pressure run (thinnest boundary layer) to data obtained late in a low pressure run (thickest boundary layer). These data are presented in Fig. 14 for each Mach number. The δ^*/d variation from one test condition to another is over 100 percent, and still the differences in cone-cylinder pressure distribution are small.

4.3 QUANTIFYING THE RESULTS

Two methods have been used to quantify the small variation in the cone-cylinder pressure distributions which appear to result from a δ^*/d change, in terms of a wall porosity and an effective wall crossflow characteristic variation. For Mach numbers above 1.1, a characteristics solution of the cone-cylinder flow field can be generated and the boundary condition at the wall established to match the experimental cone cylinder pressure distribution as reported in the appendix of Ref. 2. The calculated wall crossflow characteristic was found to decrease about 10 percent for a 40-percent increase in δ^*/d from 0.175 to 0.242 at Mach 1.15 (see Fig. 12). This is equivalent to about a one-half-percent change in porosity. This slight "apparent" change in effective porosity with δ^*/d could also be caused in part by a tunnel Mach number calibration difference of about 0.005.

For Mach numbers below those sufficient for a fully supersonic cone ($M_\infty < 1.1$) and for which a characteristics solution cannot be generated, a crossplot of the experimental results given in Ref. 3 has been used to quantify the measured variations attributed to δ^*/d changes. Figure 15 presents the data from Ref. 3 used in the crossplot. For nominal Mach numbers of 1.05, 1.075, and 1.1 the influence of a varying wall porosity on the cone-cylinder pressure distribution can be seen. Some of the data available in Ref. 3 were

not used since the ΔM between conditions was greater than 0.005 and spurious Mach number effects would be introduced. The plot of change in pressure ratio with wall porosity for the three Mach numbers is given in Fig. 16. This is taken at the point at which the maximum disturbance in the cone-cylinder pressure distribution occurs. The x/D location of the porosity sensitive local disturbance shifts with Mach number. For the data presented, this is at about the location where a wave returns which originated as the corner expansion wave (see curves Ⓑ and Ⓒ in Fig. 7).

An evaluation of the slight differences in Figs. 12, 13, and 14, where careful attention is directed toward cases with $\Delta M < 0.005$ only, reveals that the greatest measured variation in pressure distribution resulting from a δ^*/d variation of 0.13 to 0.28 is equivalent to a change in porosity of about one percent (based on Fig. 16). Most of the differences are equivalent to less than one percent $\Delta\tau_w$. Hence, as δ^*/d varies about a factor of two between 0.13 and 0.28, it appears that the effective wall porosity change is $\lesssim 1$ percent. This is also equivalent to a change in the wall crossflow characteristic of less than 15 percent. A more precise statement of the influence of δ^* could only be made after a more careful tunnel calibration. The relatively thick, but low δ^*, test section wall boundary layer associated with Ludwieg tubes does not appear to change the nature of the wall crossflow.

5.0 CONCLUSIONS

Variations in the pressure distribution on a cone-cylinder model have been evaluated as the boundary-layer displacement thickness on the test section wall of a transonic wind tunnel was varied from 0.13 to 0.28 times the wall hole diameter. The maximum observed variation in pressure distribution as a result of this δ^*/d variation is equivalent to a change in effective porosity of the wall of about one percent or less and represents a change in the wall crossflow characteristic, $dC_p/d\theta$, of about 15 percent or less. This one-percent change in apparent porosity caused by the factor of two change in δ^*/d probably represents an upper limit of the real influence of δ^* on the wall crossflow character (for $0.13 < \delta^*/d < 0.28$) when the slight but important data and tunnel calibration uncertainties are considered. Previous data indicate that more significant crossflow changes can be expected for $\delta^*/d > 0.5$.

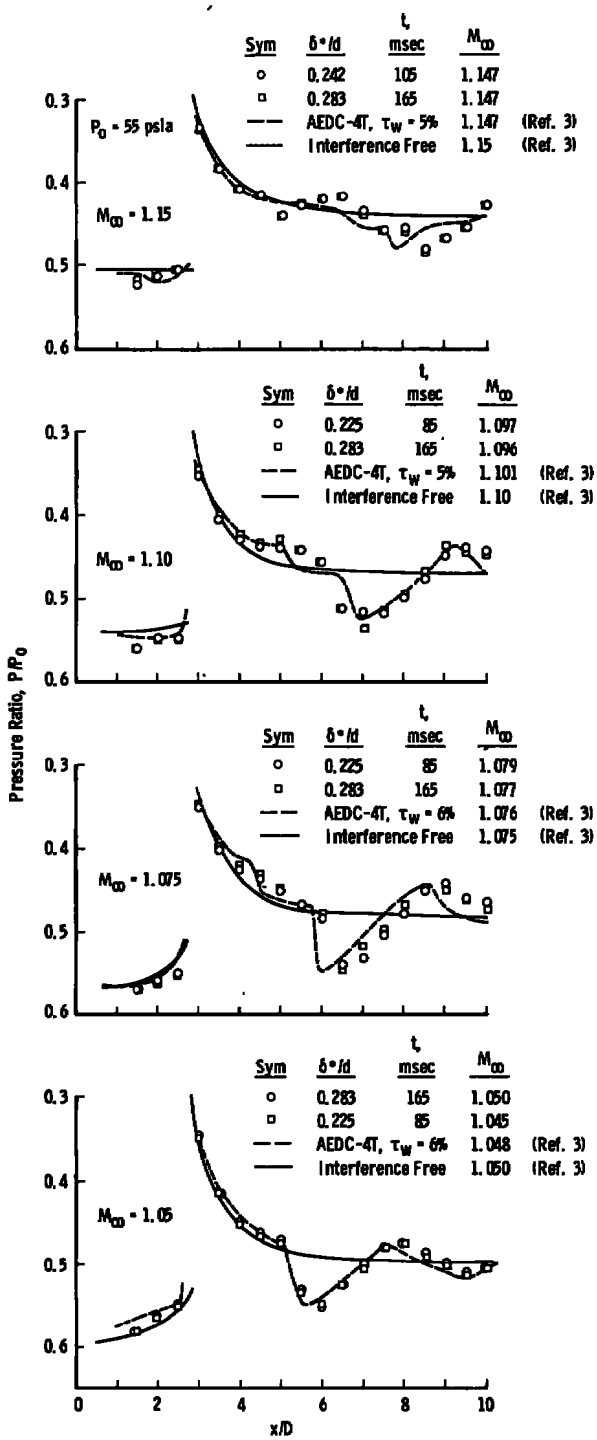

a. 55-psia stagnation pressure

Figure 13. Comparison of cone-cylinder pressure distribution data at Mach numbers of 1.05 to 1.15 at various flow times in Pilot HIRT.

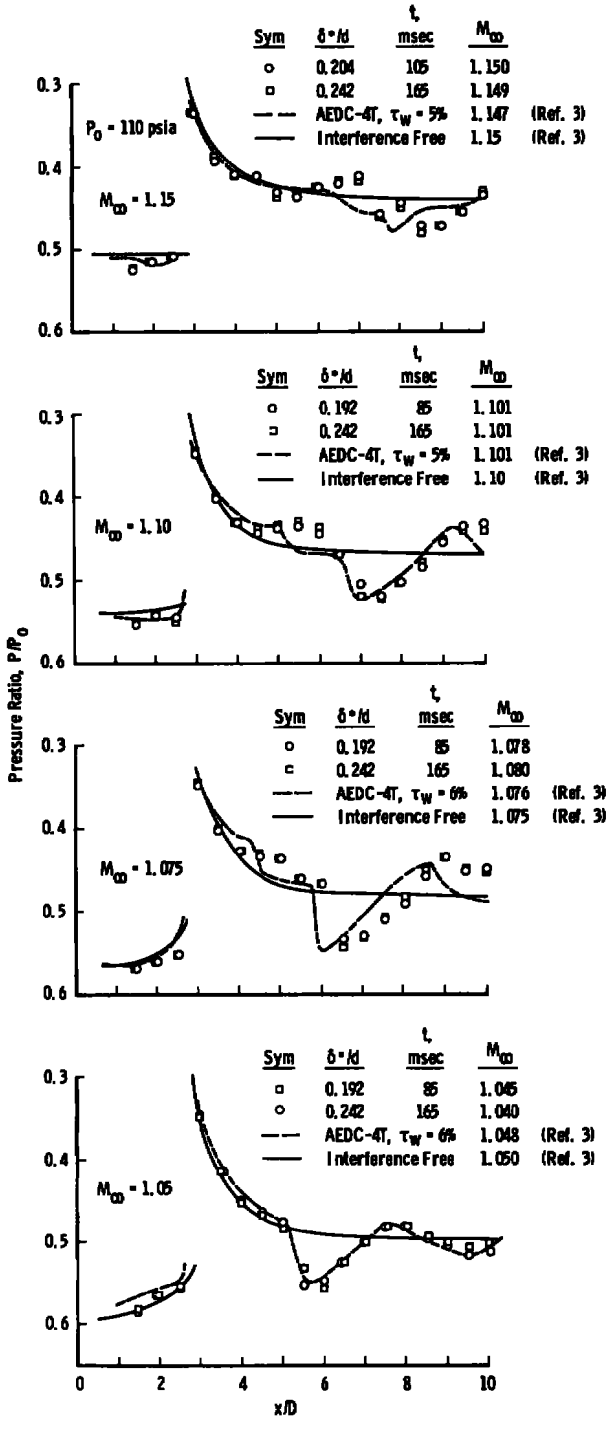

b. 110-psia stagnation pressure
Figure 13. Continued.

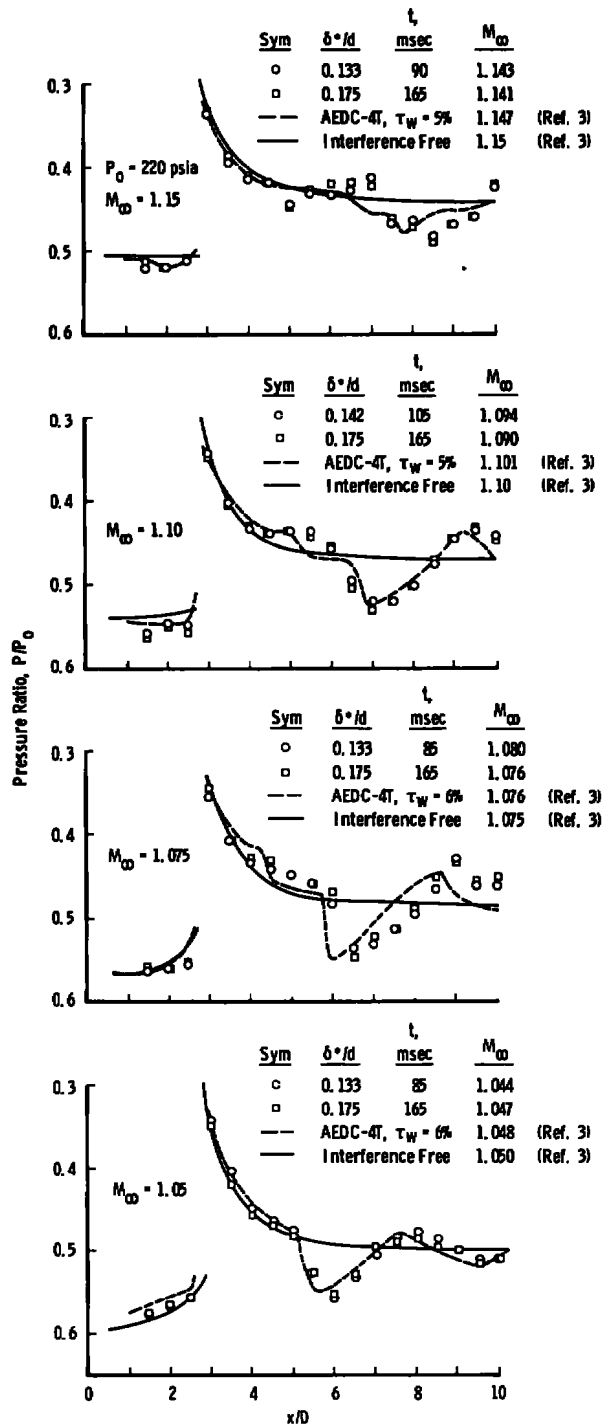

c. 220-psia stagnation pressure

Figure 13. Concluded.

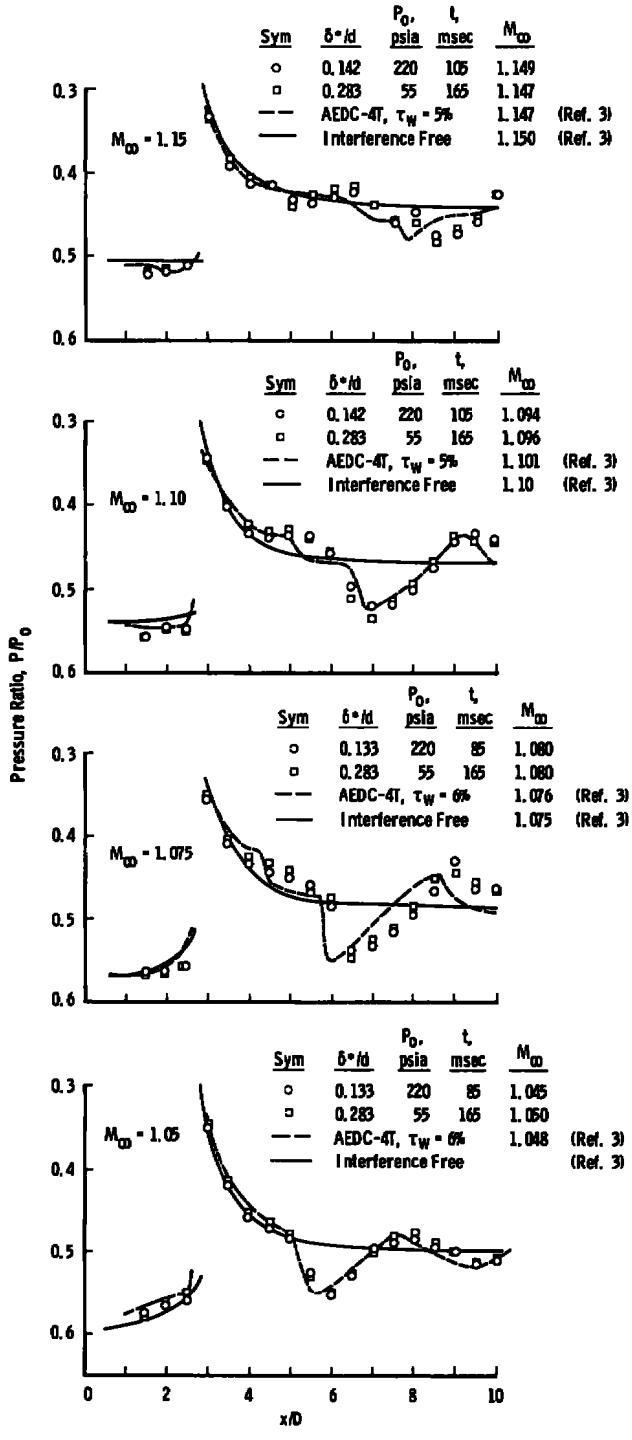

Figure 14. Cone-cylinder pressure distributions at Mach numbers of 1.05 to 1.15 for extremes of δ^*/d.

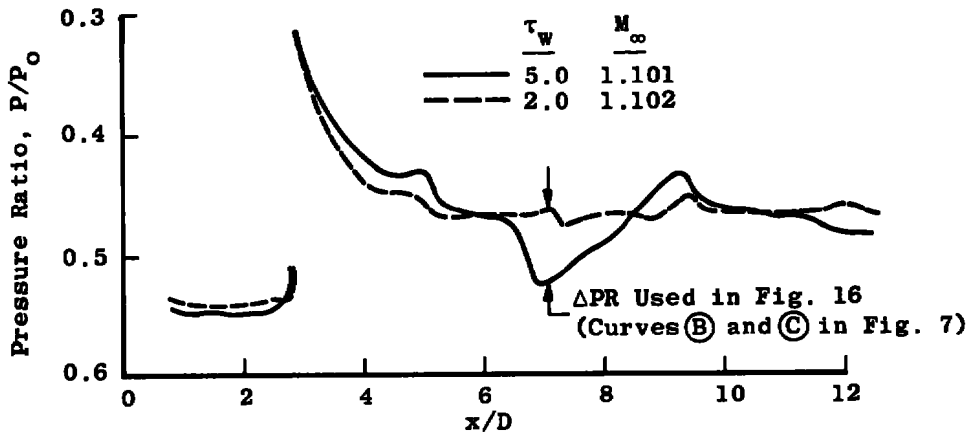

a. $M_\infty \sim 1.10$

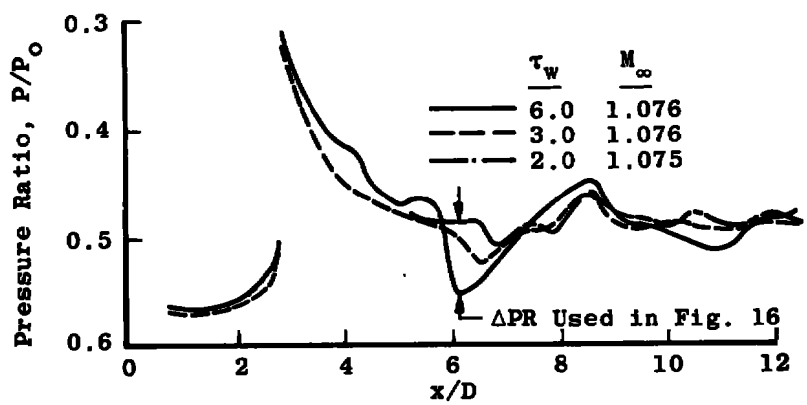

b. $M_\infty \sim 1.075$

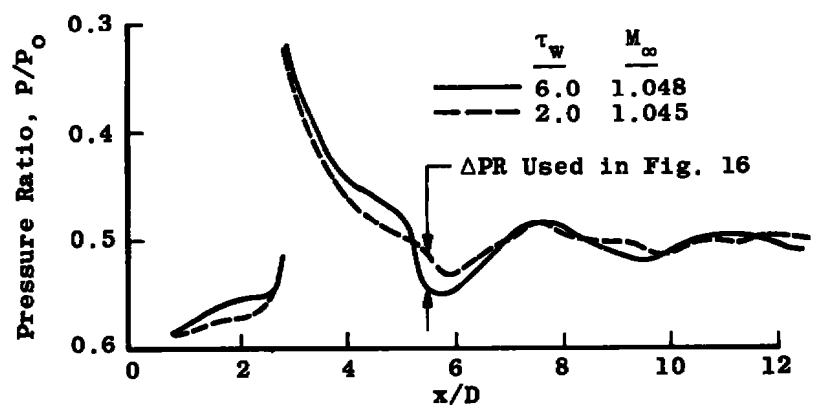

c. $M_\infty \sim 1.05$

Figure 15. Influence of varying wall porosity on cone-cylinder pressure distributions (from Ref..3).

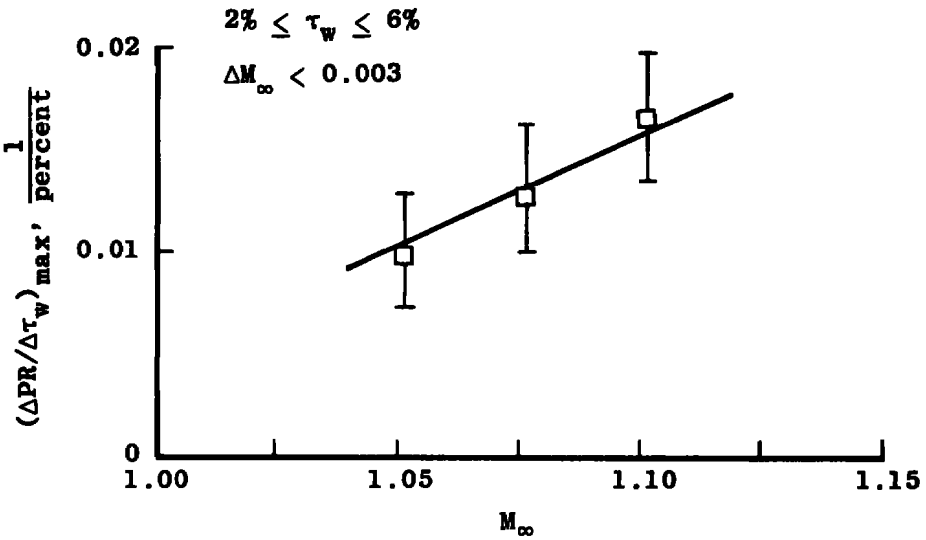

Figure 16. Change in cone-cylinder pressure ratio with porosity for Mach numbers 1.05 to 1.10.

REFERENCES

1. Goethert, B. H. Transonic Wind Tunnel Testing. Pergamon Press, Ltd., London, England, 1961 (First Edition).

2. Jacocks, J. L. "Evaluation of Interference Effects on a Lifting Model in the AEDC-PWT 4-Ft Transonic Tunnel." AEDC-TR-70-72 (AD868290), Arnold Engineering Development Center, Arnold Air Force Station, Tennessee, April 1970.

3. Jacocks, J. L. "Determination of Optimum Operating Parameters for the AEDC-PWT 4-Ft Transonic Tunnel with Variable Porosity Test Section Walls." AEDC-TR-69-164 (AD857045), Arnold Engineering Development Center, Arnold Air Force Station, Tennessee, August 1969.

4. Starr, R. F. and Schueler, C. J. "Experimental Studies of a Ludwieg Tube High Reynolds Number Transonic Tunnel." AEDC-TR-73-168 (AD771646), December 1973; also AIAA Journal, Vol. 12, No. 3, March 1974.

5. Jacocks, J. L. "Reduction of Wall Interference Effects in the AEDC-PWT 1-Ft Transonic Tunnel with Variable Perforated Walls." AEDC-TR-69-86 (AD851575), Arnold Engineering Development Center, Arnold Air Force Station, Tennessee, May 1969.

6. Estabrooks, B. B. "Wall Interference Effects on Axisymmetric Bodies in Transonic Wind Tunnels." AEDC-TR-59-12 (AD216698), Arnold Engineering Development Center, Arnold Air Force Station, Tennessee, June 1959.

NOMENCLATURE

C_p	Wall pressure coefficient, defined as a pressure drop across the wall divided by q_∞ (Ref. 1)
D	Cone-cylinder diameter (0.914 in. in Pilot HIRT)
d	Wall hole diameter (0.12 in. in Pilot HIRT)
M_p	Mach number based on measured plenum pressure
M_∞	Free-stream Mach number
$\overline{M}_\infty$	Average free-stream Mach number in the test region
P	Local static pressure, psia
P_p	Plenum static pressure, psia
P_o	Stagnation pressure, psia
P_4	Ludwieg tube charge pressure, psia
q_∞	Free-stream dynamic pressure, psia
t	Time, measured from the initial test section pressure drop, msec
x	Axial distance measured from the cone-cylinder model nose, in.
y	Vertical distance from the wall, in.
ΔM	Variation in Mach number, with time or from one condition to another
ΔP_o	Variation in stagnation pressure with time, psia
ΔP_p	Variation in plenum pressure with time, psia
$\Delta PR/\Delta\tau_w$	Slope of pressure ratio, P/P_o with wall porosity, 1/percent
δ	Boundary-layer thickness, in.

δ^* Boundary-layer displacement thickness, in. $\delta^* = \int_0^{\delta} \left(1 - \frac{\rho u}{\rho_e U_e}\right) dy$

θ Flow angle at the wall, radians; also the ratio of mass flux perpendicular to the wall to the free-stream mass flux

$\rho u/\rho_e u_e$ Ratio of local mass flux in the boundary layer to the mass flux outside of the boundary-layer edge

τ_w Test section wall porosity, percent